ACS OMEGA

http://pubs.acs.org/journal/acsodf

Article

Apoptotic Induction of Mitochondria-Anchored Aggregation-Induced Emission Luminogens through the Intrinsic Mitochondrial Pathway

Hao Zhang, Ziting Zhang, Siwan Wang, Tianzhu Qiu, Tongpeng Xu,* and Yongqian Shu*

Cite This: *ACS Omega* 2022, 7, 47912–47922

Read Online

ACCESS | Metrics & More | Article Recommendations

ABSTRACT: Gastric cancer has the third highest mortality rate globally. Chemotherapy is the primary treatment used in advanced gastric cancer. Aggregation-induced emission luminogens (AIEgens) have been exploited as non-toxic and efficient chemotherapy agents for the treatment of cancer. Our previous research demonstrated that tetraphenylethene-substituted pyridinium salt (TPE-Py) is a kind of AIEgen that had the ability to lead to apoptosis in gastric cancer cells. However, it is currently unknown whether TPE-Py induced apoptosis in gastric cancer cells by the mitochondria-mediated pathway. This research confirmed that TPE-Py could target mitochondria and induce apoptotic cell death. In addition, several well-recognized indicators were detected to investigate the functional and morphological changes of mitochondria. We found that TPE-Py could diminish the mitochondrial membrane potential and increase the accumulation of reactive oxygen species and the discharge of cytochrome *c*, which was related to the mitochondrial apoptotic pathway. Meanwhile, morphological changes in mitochondria were also observed by transmission electron microscopy in gastric cancer cells after incubation with TPE-Py. In conclusion, we provided insights into the mechanism regulating apoptosis in gastric cancer cells and elucidated the mechanism of apoptosis induced by TPE-Py *via* the intrinsic mitochondrial pathway.

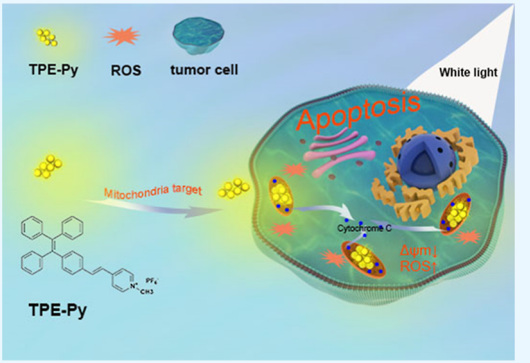

INTRODUCTION

Gastric cancer accounts for the third place in malignancy in the whole world.[1] While surgery is a potentially curative approach for localized cases, gastric cancer is highly lethal due to its late discovery, aggressive growth, and frequent metastases.[2−4] As a result, traditional chemotherapy is also the main treatment in clinics.[5] However, resistance to chemotherapy drugs has become a common cause of treatment failure in gastric cancer patients.[5−8] It is urgent to develop new therapeutic tactics to improve the prognosis and longtime survival.

Photodynamic therapy (PDT) has been recommended as a substitution therapeutic method in recent years and attracted great attention. The onset of PDT requires two components: photosensitization (PS) and light irradiation.[9] During the onset of PDT, the irradiation of a PS causes the conversion of molecular oxygen in cells and tissues into a range of reactive oxygen species (ROS), thus exerting the cytotoxic effect.[10] In this process, PDT can cause selective photodamage to malignant tissues or their vasculature. Compared with surgery, chemotherapy, and radiotherapy, PDT showed several advantages, including high specificity, controllability, and minor side effects.[9] As an essential target for PDT, mitochondria are always a hot topic.

According to reports, Oleinick 's group first confirmed that PDT can induce tumor cells to undergo apoptosis.[11] It has been reported that the majority of PDT inhibits tumors by triggering cancer cell apoptosis. Apoptosis is a programmed cell death with specific morphological and biochemical changes.[12] Many anticancer drugs induced cell death by apoptosis. Apoptosis can be triggered by two pathways, mitochondria (the intrinsic pathway) or death receptors (the extrinsic pathway).[13] It has been proved that PDT can induce apoptosis through the mitochondrial pathway.[14]

PSs are specifically irradiated for ROS generation at the target site. It minimizes the damage to the surrounding non-targeted tissues, where it remains inactive. In recent years, more and more researchers have paid attention to aggregation-induced emission luminogens (AIEgens) because of the traits of great emission efficiency in the aggregated state, high photostability, and large Stokes' shift.[15,16] Furthermore, AIEgens have been used as a

Received: September 5, 2022
Accepted: December 2, 2022
Published: December 15, 2022

https://doi.org/10.1021/acsomega.2c05761
ACS Omega 2022, 7, 47912−47922

kind of PS in cancer therapy.[9,17,18] Tetraphenylethylene (TPE) is widely used as AIE cores and has been reported to have the ability to target mitochondria with the transport of active agents into the mitochondria.[19,20] TPE-Py is one of the AIEgens with high photostability and mitochondria-targeting capacity and has been developed for cancer imaging or therapy.[21,22] Therefore, it is vital to comprehensively explore and understand the role and mechanism of apoptosis in gastric cancer cells. Yet, the antitumor molecular mechanisms of TPE-Py have not been reported before.

Our previous study demonstrated that TPE-Py ameliorated the anticancer activity of paclitaxel revulsive apoptosis in gastric cancer cells.[22] Considering the mitochondria-targeting ability of TPE-Py and the involvement of mitochondria in the intrinsic pathway, we hypothesized that TPE-Py triggers the apoptosis of gastric cancer cells by the mitochondria-mediated pathway.

Herein, we carried out a range of experiments on two kinds of gastric cancer cells to validate this conjecture.

We first explored the ability of TPE-Py on the viability of gastric cancer cells. EdU and cell viability assays were conducted to verify the anticancer ability of TPE-Py after white light irradiation. As expected, TPE-Py repressed the cell viability and proliferation of gastric cancer cells. Thus, we developed wound-healing and transwell assays to assess the ability of TPE-Py to inhibit metastasis and invasion. Besides, TPE-Py was able to target the mitochondria in gastric cancer cells selectively. Next, we analyzed the changes in mitochondria to assess whether TPE-Py aggregation in mitochondria is involved in mitochondrial dysfunction. The experimental results demonstrated that TPE-Py showed superior capacity in depolarizing the membrane potential of mitochondria, triggering ROS production, increasing the discharge of cytochrome *c* from mitochondria, and changing the morphology of mitochondria. Immunoblot analysis demonstrated that TPE-Py downregulated the expression of some antiapoptotic proteins at the mitochondria.

Overall, this study explains the potential antitumor mechanisms of TPE-Py that TPE-Py induced gastric cancer cells *via* mitochondria-dependent apoptosis. This presented a rationale for TPE-Py to be used in clinical treatment of gastric cancer afterward.

MATERIALS AND METHODS

Materials. TPE-Py (≥99.0%) was obtained from Shanghai Aladdin Biochemical Technology (Shanghai, China). RIPA lysis buffer, PBS, and ECL kit were obtained from Epizyme Biotechnology (Shanghai, China). Coomassie brilliant blue staining solution, cell mitochondria isolation kit, EdU, 4-(2-aminoethyl)-benzenesulfonyl fluoride, sodium pyrophosphate tetrabasic, 4% paraformaldehyde fix solution, crystal violet staining solution, and GreenNuc caspase-3 assay kit for live cells were obtained from Beyotime (Nanjing, China). Dimethyl sulfoxide (DMSO) was acquired from Sigma-Aldrich, China. ROS assay kit, JC-1 mitochondrial membrane potential (MMP) assay kit, LysoTracker Red DND-99 (LysoTracker), and MitoTracker Red CM-H2XRos (MitoTracker) were obtained from Yeasen Biotechnology (Shanghai, China).

Human gastric cell lines BGC-823 and SGC-7901 were obtained from the National Collection of Authenticated Cell Cultures. Penicillin−streptomycin, fetal bovine serum (FBS), RPMI 1640 medium, and trypsin were obtained from Biological Industries (Kibbutz Beit HaEmek, Israel).

Methods. *Cancer Cell Culture.* BGC-823 and SGC-7901 cells were cultured in RPMI 1640 with the addition of 10% FBS and 1% penicillin−streptomycin. These cells were incubated in a 5% carbon dioxide incubator at 37 °C.

Cell Viability Assay In Vitro. BGC-823 or SGC-7901 cells were inoculated in 96-well plates with 5000 cells per well. Different administrations of TPE-Py were incubated in 96-well plates for 2 h, followed by white light (flashlight) irradiation (2 level, 50 lumens) for 2 min and then incubation for 22 h. Finally, 10 μL of methylthiazolyl diphenyl-tetrazolium bromide was added per well and then incubated for 4 h. After that, the previous culture medium was discarded and then added 150 μL of DMSO per well. The absorbance was checked at 540 nm by a microplate reader (Tecan, Switzerland).

Transwell Assay. Tumor cells were placed in the upper chamber with the serum-free medium, and TPE-Py was added to that upper chamber with or without light. In the lower chamber, RPMI 1640 medium containing 20% FBS was placed. After treatment for 24 h, it was taken out of the room and then fixed with 4% paraformaldehyde for 20 min. After fixation, it was dyed with crystal violet for 10 min. Cotton swabs were used to wipe away the cells that did not migrate from the chamber on the membrane, and the cell migration was observed under the microscope. The migration rate was calculated as follows

$$\text{Migration rate } (\%) = \frac{\text{num}_{\text{lower}}}{\text{num}_{\text{total}}} \times 100\%$$

where $\text{num}_{\text{lower}}$ is the number of cells in the lower chamber and $\text{num}_{\text{total}}$ is the total number of input cells.

Wound-Healing Assay. The cells were cultivated in six-well plates and incubated overnight. The cells were scraped rapidly across the plates *via* the pipette tip. Photographs were taken after being treated with TPE-Py for 24 h, and semi-quantitative analysis was conducted. The percentage of wound healing was calculated using the following formula

$$\%\text{ of wound healing} = \frac{0\text{ h scratch width} - 24\text{ h scratch width}}{0\text{ h scratch width}} \times 100\%$$

Cell Proliferation Assay In Vitro. Cell proliferation was further tested by an EdU staining kit. In brief, BGC-823 and SGC-7901 cells were cultivated in a 12-well plate and cultured with 10 μM EdU for 2 h after 24 h of drug treatment. The cells were then fixed with 4% paraformaldehyde for 15 min. After that, PBS containing 0.5% Triton X-100 was replaced with 4% paraformaldehyde and incubated for 15 min. Finally, the nuclei were dyed by Hoechst 33342. The photos of EdU-labeled cells were taken using a fluorescence microscope.

Colocalization of TPE-Py with Mitochondria or Lysosomes. BGC-823 and SGC-7901 cells were cultivated in confocal dishes for 24 h, followed by the addition of TPE-Py (with or without light). After 24 h of dosing, the medium containing the drug was discarded and replaced with the medium containing a MitoTracker or a LysoTracker. The colocalization of TPE-Py with mitochondria or lysosomes was analyzed by confocal laser scanning microscopy (CLSM, Carl Zeiss LSM880). The colocalization was calculated according to the fluorescence of mitochondria-localized lysosomes.

MMP ($\Delta\psi_m$) Measurement. The cells were treated with TPE-Py for 24 h (with or without light) in confocal dishes. Briefly, following treatment, the cells were cultivated with JC-1 dye in darkness for 30 min. Then, JC-1 buffer was used to wash away the JC-1 dye. Finally, the cells were photographed using a confocal laser scanning microscope.

https://doi.org/10.1021/acsomega.2c05761
ACS Omega 2022, 7, 47912−47922

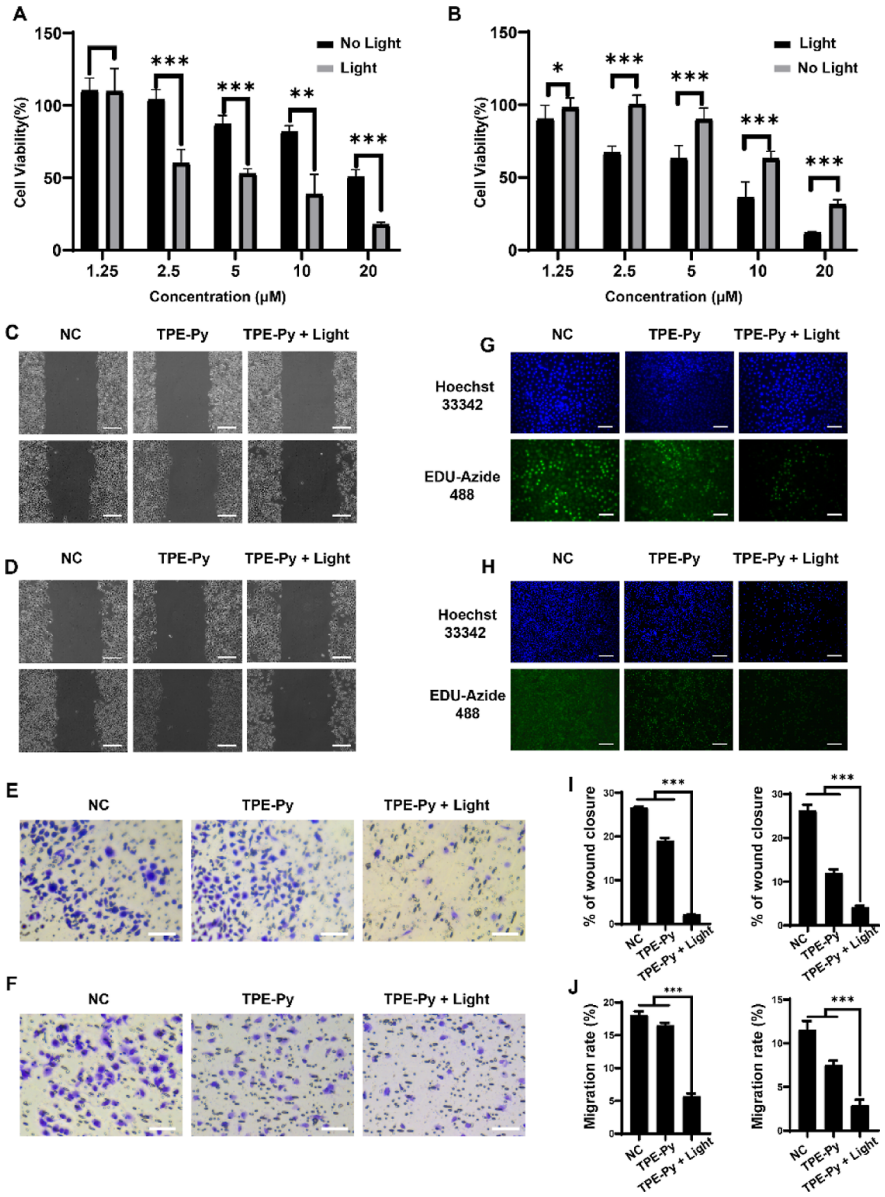

Figure 1. Cell viability, migration, and invasion of BGC-823 and SGC-7901 cells. Cell viability of BGC-823 cells (A) and SGC-7901 cells (B) after incubation with different concentrations of TPE-Py under the light. Cell migration of BGC-823 cells (C) and SGC-7901 cells (D) after being handled with different conditions, PBS, TPE-Py, and TPE-Py with light. Cell invasion of BGC-823 cells (E) and SGC-7901 cells (F) after incubation with PBS and TPE-Py with or without light. Cell proliferation of BGC-823 cells (G) and SGC-7901 cells (H) was detected by the EdU assay. Scale bar: 200 μm. Semiquantitative analysis of wound-healing assays (I) and migration assays (J) was performed by ImageJ. $n = 3$, ***$p < 0.001$.

Detection of ROS. A DCFH-DA cellular ROS detection assay (Yeasen) was used to detect the total ROS activity within the cells. After the treatment, the cells were stained in a culture medium with DCFH-DA dye for 30 min in darkness and then recorded using a confocal laser scanning microscope.

Transmission Electron Microscopy. Tumor cells were fixed with 2.5% glutaraldehyde at 4 °C. After that, the cells were dehydrated in stages with different concentrations of ethanol and then dyed with uranyl acetate and lead citrate. In the end, pictures were taken using a transmission electron microscope (JEOL, Japan).

GreenNuc Caspase 3. The cells were cultivated in confocal dishes respectively for 24 h. After that, they were treated with TPE-Py with or without light. After treatment, the GreenNuc caspase-3 substrate was mixed with the medium and replaced with the previous medium. The cells were cultivated with the dye for 30 min. Then, the medium was discarded and added 4% paraformaldehyde to fix it for 15 min. Finally, the cells were observed under a confocal laser microscope.

Isolation of Mitochondria. Cells were cultivated under different conditions for 24 h. After digestion, 1 mL of the Mitochondria Isolation Reagent was mixed for 15 min. The cells were homogenized using a glass homogenizer. The homogenate was put into a 1.5 mL centrifuge tube and centrifuged for 10 min (600*g*, 4 °C). After that, the supernatant was taken into another tube and centrifuged again for 10 min (3500*g*, 4 °C). Finally, the supernatant obtained in the previous step performed another round of centrifugation at 12,000*g* for 10 min (4 °C).

Western Blot Analysis. The protein was collected from cells treated by DMSO, TPE-Py, and TPE-Py with light for 24 h. After denaturation and reductive alkylation, equivalent quantities of protein were isolated by 10−15% SDS-PAGE and then

https://doi.org/10.1021/acsomega.2c05761
ACS Omega 2022, 7, 47912−47922

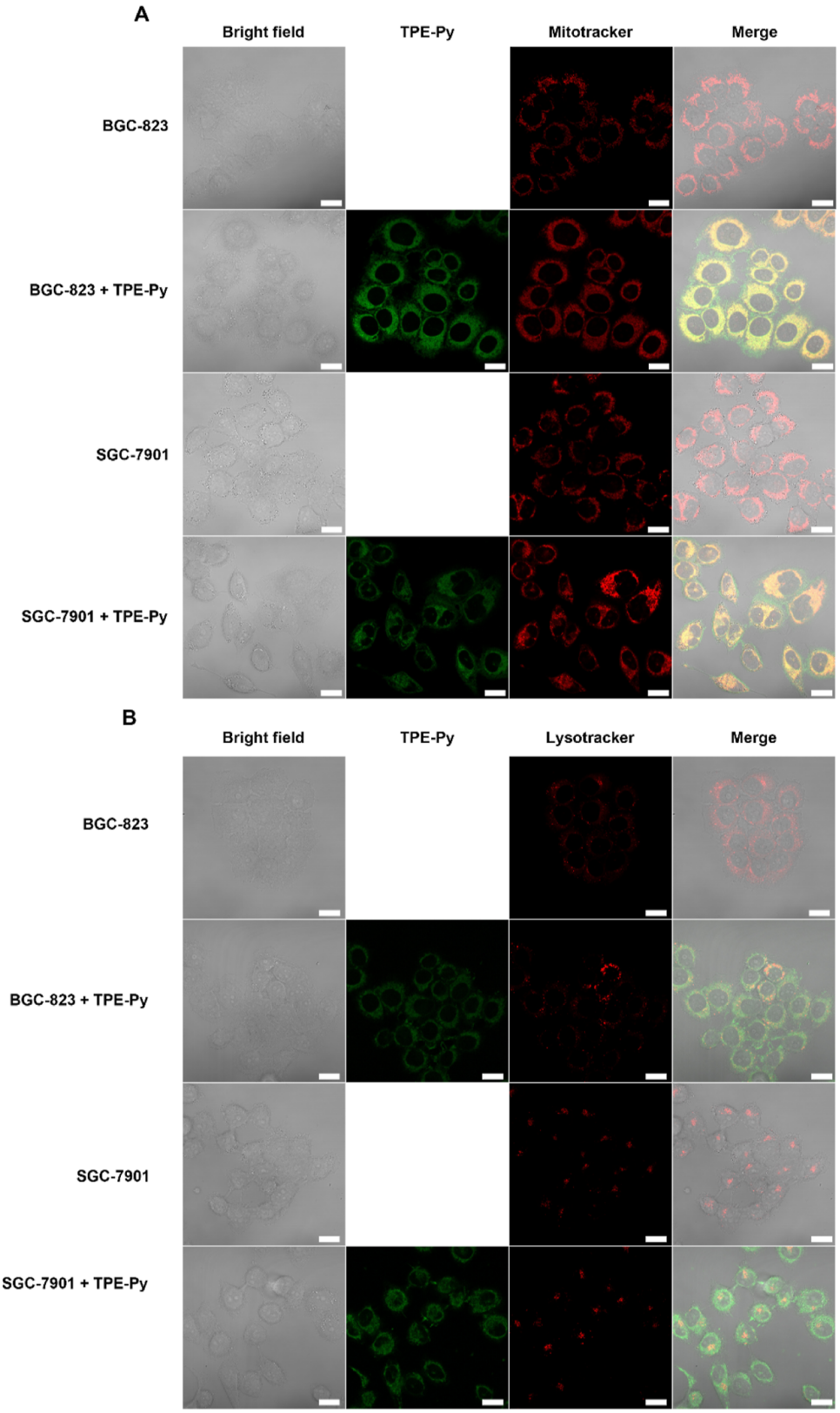

Figure 2. Confocal microscopic analysis of cellular colocalization. (A) Representative confocal microscopy images of TPE-Py (green) colocalization with the endolysosomal dye LysoTracker (red) in BGC-823 and SGC-7901 cells (A). Colocalization of TPE-Py with mitochondria is shown in yellow. (B) Confocal images of the colocalization of TPE-Py with LysoTracker Red DND-99 in BGC-823 and SGC-7901 cells (B). Colocalization of TPE-Py with the lysosome is shown as yellow. Scale bar: 2 μm.

transferred the protein to polyvinylidene difluoride membranes. Then, the polyvinylidene difluoride membranes were immersed in 5% skimmed milk for 1 h for blocking. After that, the membranes were incubated at 4 °C with primary antibodies

https://doi.org/10.1021/acsomega.2c05761
ACS Omega 2022, 7, 47912−47922

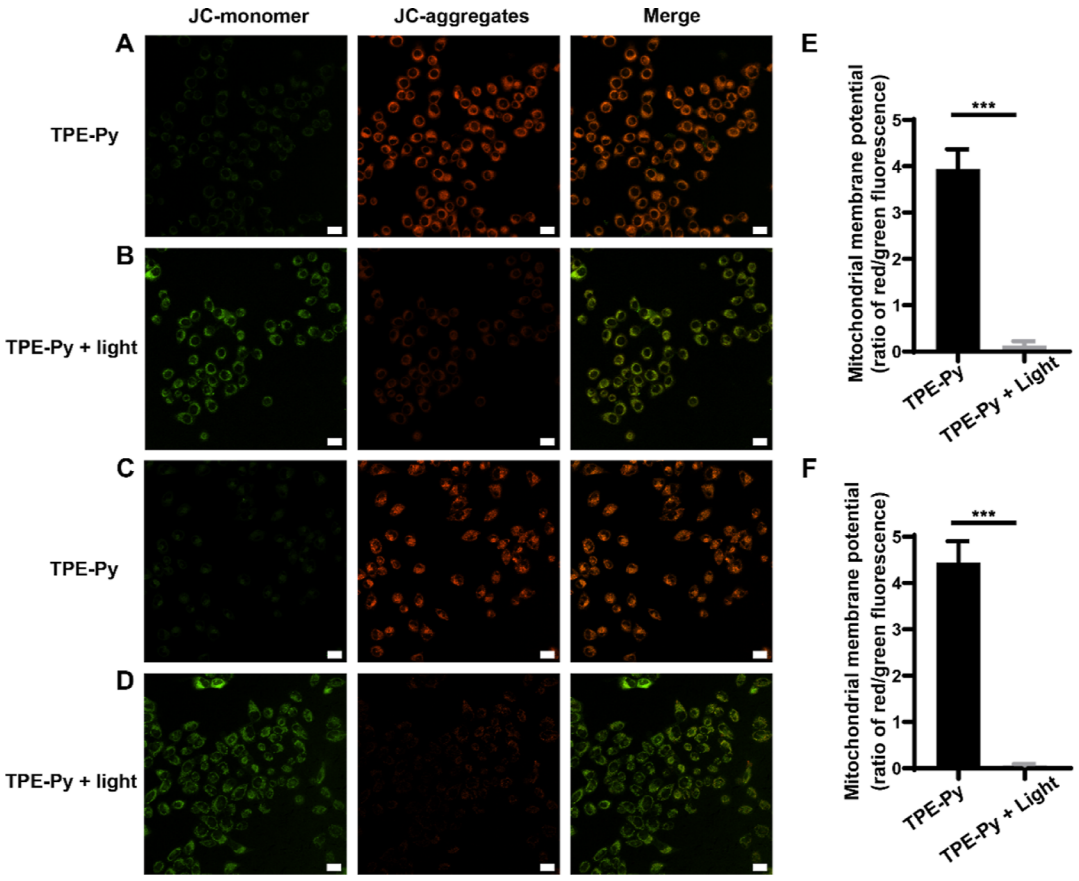

Figure 3. TPE-Py-induced mitochondrial membrane depolarization. Measurement of MMP ($\Delta\psi$) in gastric cancer cells. MMP determination on BGC-823 cells handled with TPE-Py (A) and TPE-Py with light irradiation (B). MMP determination on SGC-7901 cells treated with TPE-Py (C) and TPE-Py with light irradiation (D). Scale bar: 20 μm. Quantification data of MMP in BGC-823 cells (E) and SGC-7901 cells (F), respectively. $n = 3$, ***$p < 0.001$.

against phosphorylated Akt (p-Akt), phosphorylated Bad (p-Bad), and cytochrome *c*, and then the membranes were incubated with secondary antibodies. The protein bands were visualized in an ECL solution for 1 min, and the protein band images were taken using a Tanon-5500 chemiluminescent imaging system.

Statistical Methods. Statistical analysis data were shown as mean ± standard deviation. The statistical analyses were performed with the Student *t*-test using GraphPad Prism 7.0 (GraphPad software).

Semiquantitative analysis of fluorescence images and western blots was performed with ImageJ software (National Institutes of Health Freeware). The difference between different comparisons was deemed to be statistically significant when $p < 0.05$. *$p < 0.05$, **$p < 0.01$, and ***$p < 0.001$.

RESULTS

***In Vitro* Cytotoxicity.** The cells were handled with varying concentrations of TPE-Py (with or without light) for 24 h. Cell death was determined as mentioned above. As shown in Figure 1, various concentrations of TPE-Py could induce different extents of cell death. With increasing concentrations, the cellular viability dropped to <20% at concentrations higher than 20 μM. The IC_{50} values of TPE-Py against BGC-823 and SGC-7901 were 11.6 and 7.1 μM, separately.

Cellular growth and proliferation are highly regulated events in cancer cells. To address whether TPE-Py with irradiation influences cell proliferation, EdU was used to label the proliferating cells. After being treated for 2 h, the proliferation was examined by fluorescence microscopy. Figure 1G,H demonstrates that TPE-Py after irradiation significantly suppressed cell proliferation, as less EdU incorporation is observed at TPE-Py with light groups.

Considering metastasis is the primary reason for death in cancer patients. We then performed wound-healing and transwell assays to assess the ability of TPE-Py to inhibit metastasis and invasion. As displayed in Figure 1C,D, the migration of gastric cancer cells was markedly reduced after incubation with TPE-Py and illumination, compared to control conditions. Meanwhile, from Figure 1E,F, we found that the number of cells treated by TPE-Py with irradiation that could prevent invasion through the membrane was much less than that of the control groups or TPE-Py without light groups. The above two experiments were conducted with similar results.

In conclusion, the above results demonstrated the excellent cytotoxicity and anticancer activity of TPE-Py after light irradiation. In contrast, TPE-Py without irradiation was unable to restrain cell proliferation, metastasis, and invasion.

Subcellular Localization. Subcellular localization is crucial for assessing the efficiency and bioavailability of the agents. To investigate the mitochondria-targeting ability of TPE-Py, BGC-8223 and SGC-7901 cells were handled with TPE-Py and then dyed by a MitoTracker. Then, they were observed by a confocal laser scanning microscope.

The distribution of agents to the mitochondria of cells influences the therapeutic efficacy. As such, we first evaluated the

https://doi.org/10.1021/acsomega.2c05761
ACS Omega 2022, 7, 47912−47922

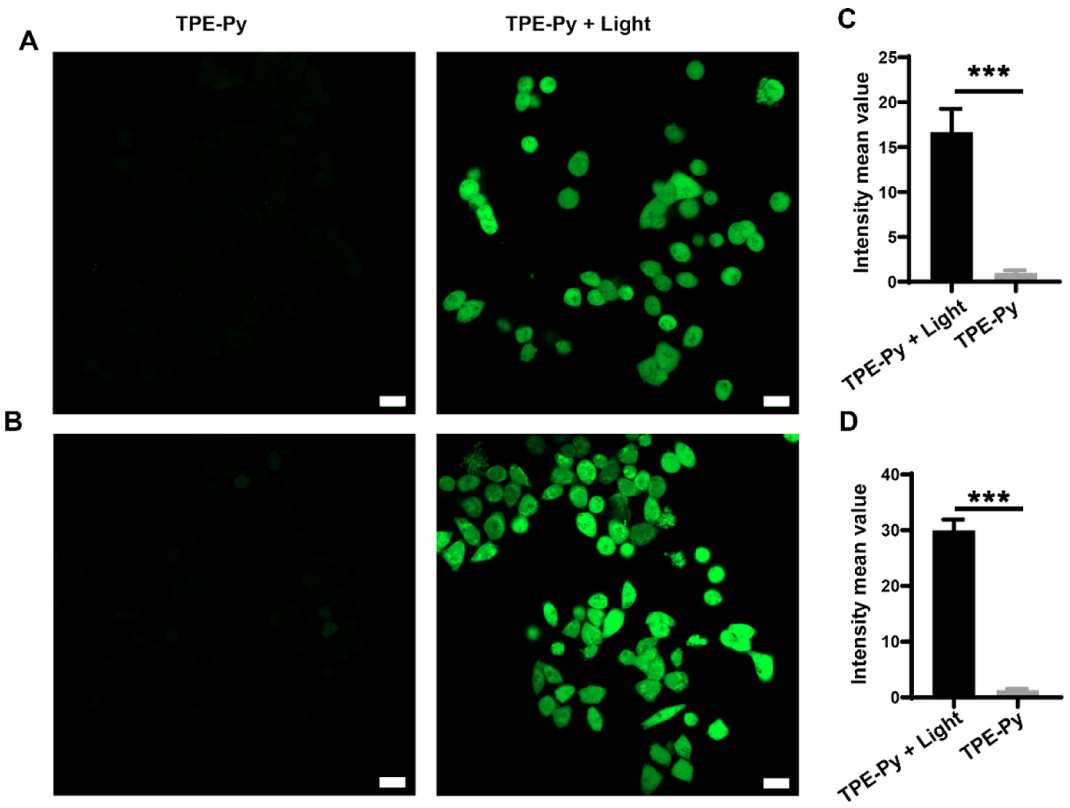

Figure 4. ROS levels in gastric cancer cells. Representative confocal images of DCFH-DA staining for ROS detection against BGC-823 (A) and SGC-7901 (B) cells. Scale bars = 20 μm. Semiquantitative analysis of cellular ROS levels in BGC-823 (C) and SGC-7901 (D) cells. $n = 3$, ***$p < 0.001$.

intracellular distribution of TPE-Py in gastric cancer cells. As displayed in Figure 2A, the merged images display the overlap of mitochondrial staining (red) and TPE-Py (green). Quantitative analysis using the ImageJ revealed the colocalization of TPE-Py with a MitoTracker in the mitochondria of cells. The overlap of the lysosome tracker (red) and TPE-Py (green) is presented in Figure 2B.

In contrast, the intracellular colocalization of the intracellular lysosome colocalization analysis exhibited a little overlap between TPE-Py with a LysoTracker, which indicated the effective endosomal escape of TPE-Py after the cellular internalization.

Pixel scattergrams and colocalization coefficients indicate that TPE-Py was more colocalized with mitochondria (Pearson's coefficient 0.82) than lysosomes (Pearson's coefficient 0.26). Therefore, TPE-Py was verified to enter the cell and then mainly localize in the mitochondria.

These results reveal that TPE-Py can be localized in mitochondria selectively, as well as lysosomal escape.

Mitochondrial Dysfunction Assay. Mitochondrial dysfunction is the key to apoptosis for effective cancer therapy. To assess whether the probe aggregation in mitochondria is involved in mitochondrial dysfunction, JC-1 (5′,6,6′-tetrachloro-1,1′,3,3′-tetraethylbenzimidazolylcarbocyanine iodide), a specific mitochondrial dye, was used to detect changes in the MMP ($\Delta\psi_m$) caused by TPE-Py. Normal MMP was higher than the abnormal one, and JC-1 formed polymers in the mitochondria and exhibited red fluorescence. When mitochondria were damaged, the MMP decreased, and JC-1 remained in a monomer state and did not gather in the mitochondria, thus showing green fluorescence. The decreased red/green fluorescence density ratio displayed mitochondrial dysfunction (Figure 3).

The results of Figure 3 demonstrated that BGC-823 and SGC-7901 cells handled with TPE-Py without light showed intense red fluorescence, indicating that their mitochondria were intact. In contrast, the weak red fluorescence and strong green fluorescence after treatment with TPE-Py with light irradiation suggest severe damage to mitochondria.

Generation of ROS. As shown in Figure 4A,B, cells handled with TPE-Py and light irradiation exhibited stronger green fluorescence than those incubated with TPE-Py without illumination. We found an increase in mitochondrial ROS production after white light irradiation through semiquantitative analysis of the fluorescence intensity (Figure 4C,D).

TPE-Py treatment with light groups caused a noticeable increase in ROS levels, while the TPE-Py groups, as a comparison, showed a much lower fluorescence intensity.

These results showed that TPE-Py has excellent photodynamic activity under white light irradiation.

Mitochondria Injury Monitoring. One of the decisive manifestations of intrinsic apoptosis progression is the changes in mitochondrial morphology. We used transmission electron microscopy (TEM) to monitor the morphological changes in mitochondria.

The TEM images in Figure 5 showed that compared with control and TPE-Py without irradiation groups, most mitochondria in TPE-Py and irradiation groups showed a decreased mitochondrial area and perimeter. Moreover, the cristae of mitochondria almost wholly disappeared in gastric cancer cells. Meanwhile, the mitochondrial matrix showed fragmentation, swelling, and vacuoles. These results reveal that

https://doi.org/10.1021/acsomega.2c05761
ACS Omega 2022, 7, 47912−47922

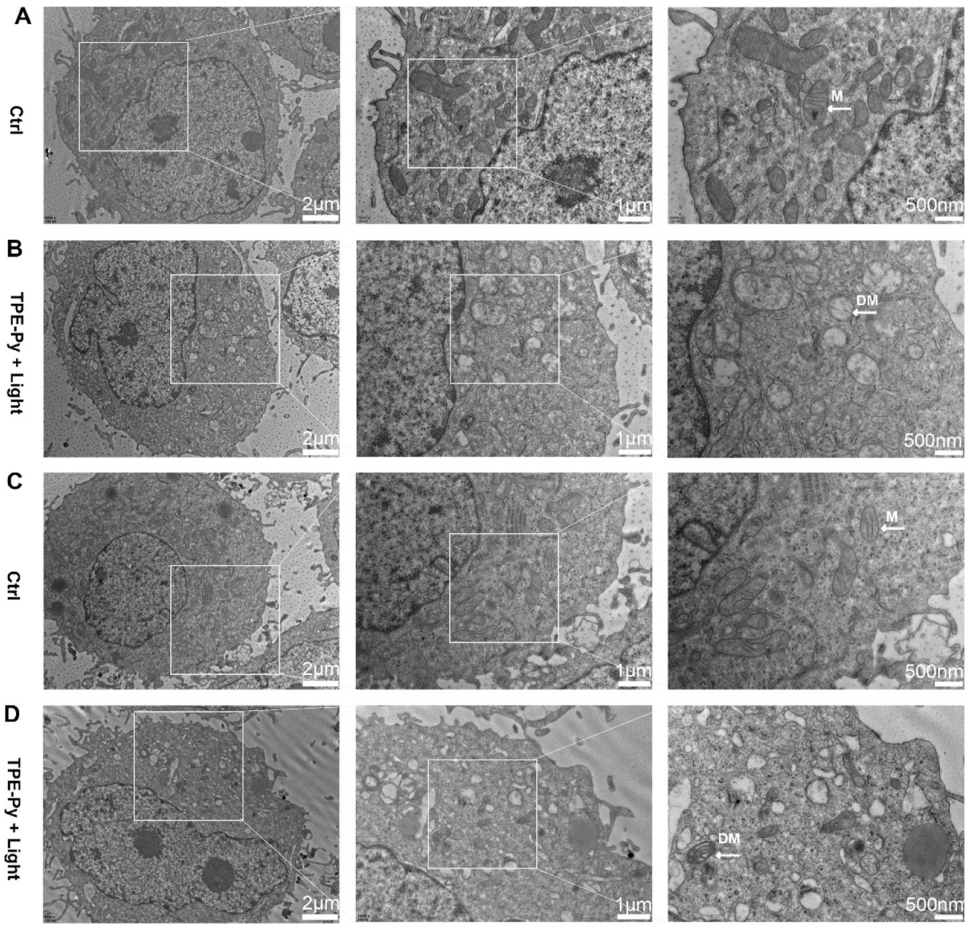

Figure 5. Mitochondria injury monitored by TEM. (A,B) Representative images of BGC-823 cells without any treatment or treatment with "TPE-Py + light". (C,D) Representative images of SGC-7901 cells without any treatment or treatment with "TPE-Py + light". The mitochondria and damaged mitochondria were labeled M and DM, respectively. Scale bars (2 μm, 1 μm, and 500 nm) are shown in the images.

TPE-Py with irradiation disrupted the mitochondrial morphology.

Analysis of Mitochondrial Proteins. As to the mechanism of cell death, we tested activated caspase 3, a marker of programmed cell death. The caspase 3 activity was tested by a GreenNuc caspase-3 assay kit. While cells undergo apoptosis, caspase-3 is activated and then cleaves the GreenNuc caspase-3 substrate. Then, the DNA dye was released to bind with DNA and yield a fluorescent signal. The representative images in Figure 6A were acquired using CLSM. As can be seen, the green fluorescence intensity of activated caspase 3 cells was significantly higher in TPE-Py with irradiation groups than that of TPE-Py without irradiation groups. Briefly, we observed apparent apoptosis in TPE-Py with light groups than without light groups. The results suggest that TPE-Py induced early apoptosis because caspase 3 is an early apoptotic marker.

To verify the activation of the apoptotic signaling pathway, we also tested the expression levels of the apoptosis-related protein, including cytosolic cytochrome *c* (Cyt *c*), p-Akt, and p-Bad. As shown in Figure 6C, compared with the control groups, p-Akt and p-Bad proteins both decreased significantly in two gastric cancer cells after incubation with TPE-Py and illumination. The experimental groups exhibited more Cyt *c* release after irradiation than the control groups. Meanwhile, the release of Cyt *c* from mitochondria to cytosol increased.

Figure 6 displays that the pro-apoptosis protein caspase 3 was upregulated, while the antiapoptosis proteins were markedly downregulated under light irradiation. Meanwhile, cytochrome *c* was verified to release from the mitochondria to the cytosol. These results proved that TPE-Py could efficiently activate intrinsic apoptosis *via* the Akt/Bad signal pathway in gastric cancer cells.

DISCUSSION

Apoptosis is a form of energy-dependent programmed cell death. Mitochondrial apoptosis is a major apoptotic pathway.[13] It was reported that apoptosis causes uncoupling of electron transport from ATP synthesis in the mitochondria, thereby resulting in an increase in ROS, a dysfunction of the mitochondrial respiratory chain, and a decrease in transmembrane potential.[12,23]

Compared to other therapeutics, PDT is non-invasive, highly specific, and controllable. PS is an essential component of PDT. Mitochondria-targeted PSs could significantly enhance the efficiency of photodynamics because mitochondria are the sources of energy.[24] As reported previously, mitochondria-targeting AIEgens are usually lipophilic and cationic.[15,17] TPE-Py possessed both of these properties and was previously reported to be an excellent candidate in targeting the mitochondria.[21,25] Since its first synthesis, numerous studies have focused on superior aggregation-induced emission and imaging ability of TPE-Py.[21,25,26] In contrast, no previous study has investigated the antitumor efficacy of TPE-Py before our group.

https://doi.org/10.1021/acsomega.2c05761
ACS Omega 2022, 7, 47912−47922

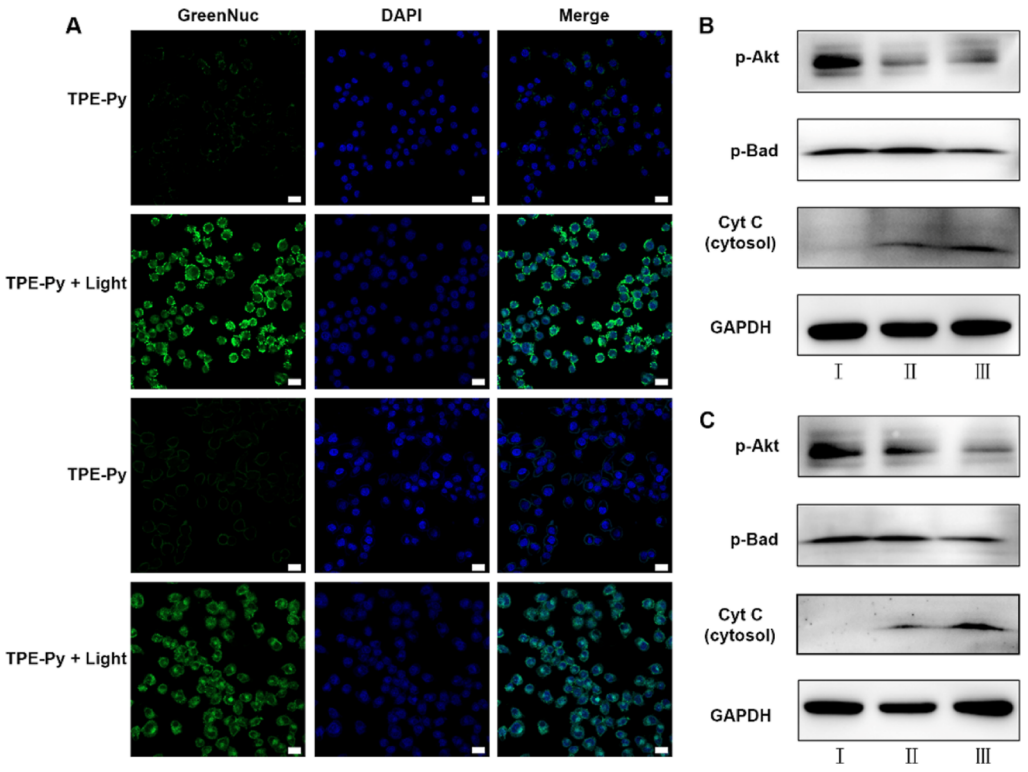

Figure 6. Analysis of mitochondria-mediated apoptosis proteins. (A) BGC-823 and SGC-7901 cells were handled under various conditions to caspase 3 to evaluate cell apoptosis. (B,C) Western blot characterized mitochondria-associated proteins under different treatments: I, control, II, TPE-Py, and III, TPE-Py + light. Scale bar: 20 μm.

Our group has reported that TPE-Py improved the anticancer activity of paclitaxel-induced apoptosis in gastric cancer cells.[22] However, we just examined its ability to trigger apoptosis. The concrete therapeutic mechanism remains unclear. Based on this premise, we further investigate the mechanism of TPE-Py-induced tumor cell apoptosis.

Briefly, this study verifies the mitochondria-targeting ability of TPE-Py and characterizes cellular and molecular changes in gastric cancer cells after being treated with "TPE-Py + light".

Unrestrained cell proliferation, migration, and invasion are typical biological characteristics of cancers, leading to metastasis, poor prognosis, and high mortality rates. We evaluated the anticancer ability of TPE-Py first. The data in Figure 1 shows that the proportion of cells undergoing apoptosis increased after incubation with TPE-Py and illumination. Considering that gastric cancer is highly aggressive with a poor prognosis,[8,27] we evaluated the antimetastatic and anti-invasive ability of TPE-Py. The representative images and statistical analysis of migration and invasion showed that TPE-Py had the ability to repress the motility of gastric cancer cells. Meanwhile, we analyzed the proliferation ability of cells after being cultivated with TPE-Py and "TPE-Py + light" by the EdU assay. Collectively, "TPE-Py + light" significantly inhibits tumor cell growth and proliferation. As we already know, no publications have investigated the impact of TPE-Py in antitumors before us.

Additionally, we explore the mechanism of TPE-Py-induced mitochondrial apoptosis. A hallmark of intrinsic apoptosis is the breakdown of the mitochondrial network. Therefore, the mitochondrion has always been regarded as an ideal target to improve PDT efficiency. TPE-Py has been reported to target the mitochondria. Thus, we verified the colocalization of TPE-Py with mitochondria, as shown in Figure 2A. Since cancer cells' MMP is more negative than that of normal cells, TPE-Py can selectively amass in the mitochondria of cancer cells. As expected, TPE-Py selectively targeted the mitochondria and was finally located in the membrane of mitochondria. The results were consistent with previous studies.[21,22] Then, we evaluated the colocalization of TPE-Py with lysosomes. As shown in Figure 2B, there is almost no overlap between TPE-Py and the lysosome, which indicates that TPE-Py can escape from the lysosome. These results demonstrate that the probe exhibits better selectivity for mitochondria in gastric cancer cells. Next, we detected MMP change to verify the mitochondrial dysfunction induced by TPE-Py with light. JC-1 was used as a membrane-potential-sensitive probe. The "TPE-Py + light" groups exhibited bright green fluorescence, while weak red fluorescence indicates severe injuries in the mitochondria of gastric cancer cells. By contrast, the "TEP-Py" groups showed a strong red fluorescence intensity, which suggests the integrity of the mitochondrial membrane. It was known that ROS is essential in PDT. The generation of ROS was closely related to apoptosis. Mitochondrial abnormalities accelerate the production of ROS and facilitate this process. The above results were consistent with the results of other studies focused on AIEgen-induced cell death.[17,28]

In addition, we further explored the mechanism in protein levels. The decrease of MMP is the trait of early apoptosis in the process of apoptosis, which triggers the mitochondria-mediated apoptosis pathway. TPE-Py can reduce the MMP (Figure 2) and then change the mitochondrial outer membrane permeability (MOMP), so the apoptosis induced by TPE-Py is coupled with the release of Cyt *c* (Figure 6). Activation of the intrinsic pathway was reported to lead to MOMP, which causes the discharge of mitochondria cytochrome *c*.[29,30] In this process, the

https://doi.org/10.1021/acsomega.2c05761
ACS Omega 2022, 7, 47912−47922

mitochondrial membrane breaks down. The MOMP is changed by pro-apoptotic signaling proteins, causing a decrease in MMP, followed by the discharge of Cyt *c* into the cytoplasm.[30,31] As reported, the discharge of Cyt *c* from the mitochondria is the main part of Bcl-2 regulating apoptosis. Cyt *c* binds to APAF-1 and then induces activation of the caspase 3-dependent apoptosis cascade. Our results showed that "TPE-Py + light" restrained the expression of p-Akt and p-Bad. Akt plays a central role in cell survival, and Bad is a downstream target for Akt. Akt causes phosphorylation of Bad at Ser136, which forms a complex with 14-3-3 protein in the cytoplasm.[32,33] As a result, this prevents Bad from connecting to Bcl-2/Bcl-xL, accelerating the stability of the mitochondrial membrane system.[33] Bad, a heterodimeric partner of Bcl-xL and Bcl-2, acts as a proapoptotic Bcl-2 family protein. It works to sequester the antiapoptotic Bcl-2 *via* dimerization.[32] Akt phosphorylation is an essential step in preventing apoptosis,[34] and downregulating p-Akt means the activation of apoptosis.[35] Bad phosphorylation is a significant segment in preserving the completeness of mitochondrial membrane systems.[33,34,36] Bad was reported to induce cell death without phosphorylation, may form heterodimers with Bcl-xL, and produce BAX homodimer.[32] Thus, reducing levels of p-Bad would also promote apoptosis.[37]

Overall, TPE-Py, as a PS, is capable of inhibiting gastric cancer *in vitro*. Notably, mitochondrial targeting plays crucial and multifaceted roles. Our study provides strong evidence that TPE-Py activates the intrinsic apoptosis pathway in gastric cancer cells.

Although our research reveals the mechanism of TPE-Py first, it has several limitations. First, this study is unable to contain the entire mechanism of the mitochondrial apoptotic pathway. More experiments will be needed to clarify its mechanism of action fully. Second, though *in vitro* assays demonstrate a mechanism of TPE-Py-induced intrinsic apoptosis, additional *in vivo* studies are required to confirm this finding. We are currently working on performing *in vivo* experiments.

The principal theoretical implication of this study is that we clarify the mechanism of TPE-Py-induced cell death. AIEgen nanoparticles with highly targeting properties are significant for the specificity and selectivity in cancer imaging and therapy. This study suggests that more attention should be taken to AIEgens inducing cell death. Both imaging properties and cytotoxicity of AIEgens should be considered. In addition, if the AIEgens are designed to target mitochondria and induce mitochondria-dependent apoptosis, the efficiency of PDT may be enhanced markedly. Meanwhile, as reported, AIEgens show great potential in imaging-guided therapy applications.[18] As in our previous studies, AIEgens have properties in chemosensitization and radiosensitizations.[17,22] Future studies may need to design more AIEgens to selectively target the mitochondria and enhance PDT, chemotherapy, and radiotherapy approaches.

In summary, this study suggests several directions for future research. First, further investigations are needed to explore the mechanisms behind AIEgen-induced cell death in cancer therapies. Second, it is crucial to design or synthesize locus-specific targeting AIEgens or AIE nanoparticles. Third, the following efforts should be devoted to developing more effective AIEgens to enhance the therapeutic efficacy, such as chemosensitization or radiosensitization. We predict that future development in AIEgens will integrate imaging with therapeutics, including photothermal therapy, photothermal therapy, chemosensitization, and radiosensitization, to demonstrate their great potential for clinical diagnosis and treatment fully.

CONCLUSIONS

In conclusion, we focus on the molecular mechanism of TPE-Py-induced apoptosis. As far as we know, the mechanism of TPE-Py has not been reported. We carried out a series of experiments. These findings showed that TPE-Py could selectively target and accumulate in the mitochondria, leading to its permeabilization, matrix swelling, and MMP loss. Meanwhile, "TPE-Py + light" induced cytochrome *c* discharge from the mitochondria to the cytosol and downregulated intrinsic apoptosis-related proteins in gastric cancer cells. We have proposed a promising mechanism of TPE-Py-induced apoptosis in PDT for gastric cancer treatment. Our findings in the current study fill a knowledge gap in the therapeutic mechanism of TPE-Py and promote its development for further clinical applications.

AUTHOR INFORMATION

Corresponding Authors

Tongpeng Xu − *Department of Oncology, First Affiliated Hospital of Nanjing Medical University, Nanjing 210029 Jiangsu, China*; orcid.org/0000-0002-6824-0276; Email: tongpeng_xu_njmu@163.com

Yongqian Shu − *Department of Oncology, First Affiliated Hospital of Nanjing Medical University, Nanjing 210029 Jiangsu, China*; Email: shuyongqian@csco.org.cn

Authors

Hao Zhang − *Department of Oncology, First Affiliated Hospital of Nanjing Medical University, Nanjing 210029 Jiangsu, China*

Ziting Zhang − *Department of Geriatrics, First Affiliated Hospital of Nanjing Medical University, Nanjing 210029 Jiangsu, China*

Siwan Wang − *Department of Pharmaceutics, School of Pharmacy, Nanjing Medical University, Nanjing 211166 Jiangsu, China*

Tianzhu Qiu − *Department of Oncology, First Affiliated Hospital of Nanjing Medical University, Nanjing 210029 Jiangsu, China*

Complete contact information is available at: https://pubs.acs.org/10.1021/acsomega.2c05761

Author Contributions

H.Z., Z.Z., and S.W. contributed equally to this work. H.Z. contributed to writing original draft, writing review and editing, and conceptualization. Z.Z. contributed to methodology, data curation, and investigation. S.W. contributed to formal analysis and data curation. T.Q. contributed to investigation. T.X. contributed to investigation, data curation, and editing. Y.S. contributed to resources, supervision, and editing.

Notes

The authors declare no competing financial interest.

ACKNOWLEDGMENTS

This study was supported by the Jiangsu Province 333 High Level Talents Project (T.X.), the Natural Science Foundation of Jiangsu Province (BK20211381 to T.X.), the National Natural Science Foundation of China (82172889 to Y.S.), and the Social Development-Key Program-Clinical Frontier Technology of Jiangsu Province (BE2020783 to Y.S.).

https://doi.org/10.1021/acsomega.2c05761
ACS Omega 2022, 7, 47912−47922

REFERENCES

(1) Sung, H.; Ferlay, J.; Siegel, R. L.; Laversanne, M.; Soerjomataram, I.; Jemal, A.; Bray, F. Global Cancer Statistics 2020: GLOBOCAN Estimates of Incidence and Mortality Worldwide for 36 Cancers in 185 Countries. *Ca-Cancer J. Clin.* **2021**, *71*, 209−249.

(2) Xie, L.; Cai, L.; Wang, F.; Zhang, L.; Wang, Q.; Guo, X. Systematic Review of Prognostic Gene Signature in Gastric Cancer Patients. *Front. Bioeng. Biotechnol.* **2020**, *8*, 805.

(3) Shah, M. A.; Jhawer, M.; Ilson, D. H.; Lefkowitz, R. A.; Robinson, E.; Capanu, M.; Kelsen, D. P. Phase II study of modified docetaxel, cisplatin, and fluorouracil with bevacizumab in patients with metastatic gastroesophageal adenocarcinoma. *J. Clin. Oncol.* **2011**, *29*, 868−874.

(4) Böger, C.; Krüger, S.; Behrens, H. M.; Bock, S.; Haag, J.; Kalthoff, H.; Röcken, C. Epstein-Barr virus-associated gastric cancer reveals intratumoral heterogeneity of PIK3CA mutations. *Ann. Oncol.* **2017**, *28*, 1005−1014.

(5) Yuan, L.; Xu, Z. Y.; Ruan, S. M.; Mo, S.; Qin, J. J.; Cheng, X. D. Long non-coding RNAs towards precision medicine in gastric cancer: early diagnosis, treatment, and drug resistance. *Mol. Cancer* **2020**, *19*, 96.

(6) Caiado, F.; Maia-Silva, D.; Jardim, C.; Schmolka, N.; Carvalho, T.; Reforço, C.; Faria, R.; Kolundzija, B.; Simões, A. E.; Baubec, T.; Vakoc, C. R.; da Silva, M. G.; Manz, M. G.; Schumacher, T. N.; Norell, H.; Silva-Santos, B. Lineage tracing of acute myeloid leukemia reveals the impact of hypomethylating agents on chemoresistance selection. *Nat. Commun.* **2019**, *10*, 4986.

(7) YiRen, H.; YingCong, Y.; Sunwu, Y.; Keqin, L.; Xiaochun, T.; Senrui, C.; Ende, C.; XiZhou, L.; Yanfan, C. Long noncoding RNA MALAT1 regulates autophagy associated chemoresistance via miR-23b-3p sequestration in gastric cancer. *Mol. Cancer* **2017**, *16*, 174.

(8) Zhou, C.; Yi, C.; Yi, Y.; Qin, W.; Yan, Y.; Dong, X.; Zhang, X.; Huang, Y.; Zhang, R.; Wei, J.; Ali, D. W.; Michalak, M.; Chen, X. Z.; Tang, J. LncRNA PVT1 promotes gemcitabine resistance of pancreatic cancer via activating Wnt/beta-catenin and autophagy pathway through modulating the miR-619-5p/Pygo2 and miR-619-5p/ATG14 axes. *Mol. Cancer* **2020**, *19*, 118.

(9) Zhang, L.; Li, Y.; Che, W.; Zhu, D.; Li, G.; Xie, Z.; Song, N.; Liu, S.; Tang, B. Z.; Liu, X.; Su, Z.; Bryce, M. R. AIE Multinuclear Ir(III) Complexes for Biocompatible Organic Nanoparticles with Highly Enhanced Photodynamic Performance. *Adv. Sci.* **2019**, *6*, 1802050.

(10) You, Q.; Zhang, K.; Liu, J.; Liu, C.; Wang, H.; Wang, M.; Ye, S.; Gao, H.; Lv, L.; Wang, C.; Zhu, L.; Yang, Y. Persistent Regulation of Tumor Hypoxia Microenvironment via a Bioinspired Pt-Based Oxygen Nanogenerator for Multimodal Imaging-Guided Synergistic Phototherapy. *Adv. Sci.* **2020**, *7*, 1903341.

(11) Agarwal, M. L.; Clay, M. E.; Harvey, E. J.; Evans, H. H.; Antunez, A. R.; Oleinick, N. L. Photodynamic therapy induces rapid cell death by apoptosis in L5178Y mouse lymphoma cells. *Cancer Res.* **1991**, *51*, 5993−5996.

(12) Burke, P. J. Mitochondria, Bioenergetics and Apoptosis in Cancer. *Trends Cancer* **2017**, *3*, 857−870.

(13) Martinou, J. C.; Youle, R. J. Mitochondria in apoptosis: Bcl-2 family members and mitochondrial dynamics. *Dev. Cell* **2011**, *21*, 92−101.

(14) Tang, P. M.; Zhang, D. M.; Xuan, N. H.; Tsui, S. K.; Waye, M. M.; Kong, S. K.; Fong, W. P.; Fung, K. P. Photodynamic therapy inhibits P-glycoprotein mediated multidrug resistance via JNK activation in human hepatocellular carcinoma using the photosensitizer pheophorbide a. *Mol. Cancer* **2009**, *8*, 56.

(15) Chen, Y.; Lam, J. W. Y.; Kwok, R. T. K.; Liu, B.; Tang, B. Z. Aggregation-induced emission: fundamental understanding and future developments. *Mater. Horiz.* **2019**, *6*, 428−433.

(16) Hong, Y.; Lam, J. W.; Tang, B. Z. Aggregation-induced emission. *Chem. Soc. Rev.* **2011**, *40*, 5361−5388.

(17) Yu, C. Y. Y.; Xu, H.; Ji, S.; Kwok, R. T.; Lam, J. W.; Li, X.; Krishnan, S.; Ding, D.; Tang, B. Z. Mitochondrion-Anchoring Photosensitizer with Aggregation-Induced Emission Characteristics Synergistically Boosts the Radiosensitivity of Cancer Cells to Ionizing Radiation. *Adv. Mater.* **2017**, *29*, 1606167.

(18) Xu, W.; Lee, M. M. S.; Nie, J. J.; Zhang, Z.; Kwok, R. T. K.; Lam, J. W. Y.; Xu, F. J.; Wang, D.; Tang, B. Z. Three-Pronged Attack by Homologous Far-red/NIR AIEgens to Achieve 1+1+1>3 Synergistic Enhanced Photodynamic Therapy. *Angew. Chem.* **2020**, *59*, 9610−9616.

(19) Chen, C.; Song, Z.; Zheng, X.; He, Z.; Liu, B.; Huang, X.; Kong, D.; Ding, D.; Tang, B. Z. AIEgen-based theranostic system: targeted imaging of cancer cells and adjuvant amplification of antitumor efficacy of paclitaxel. *Chem. Sci.* **2017**, *8*, 2191−2198.

(20) Zhang, T.; Li, Y.; Zheng, Z.; Ye, R.; Zhang, Y.; Kwok, R. T. K.; Lam, J. W. Y.; Tang, B. Z. In Situ Monitoring Apoptosis Process by a Self-Reporting Photosensitizer. *J. Am. Chem. Soc.* **2019**, *141*, 5612−5616.

(21) Zhao, N.; Li, M.; Yan, Y.; Lam, J.; Zhang, Y.; Zhao, Y.; Wong, K.; Tang, B. Tetraphenylethene-Substituted Pyridinium Salt with Multiple Functionalities: Synthesis, Stimuli-Responsive Emission, Optical Waveguide and Specific Mitochondrion Imaging. *J. Mater. Chem. C* **2013**, *1*, 4640−4646.

(22) Wang, J.; Zhang, W.; Wu, T.; Wu, H.; Zhang, Y.; Wang, S.; Ji, Y.; Jiang, H.; Zhang, Z.; Chunming, T.; Tang, Q.; Li, X.; Xu, H. Photodynamic antitumor activity of aggregation-induced emission luminogens as chemosensitizers for paclitaxel by concurrent induction of apoptosis and autophagic cell death. *Mater. Chem. Front.* **2021**, *5*, 3448−3457.

(23) Zorov, D. B.; Juhaszova, M.; Sollott, S. J. Mitochondrial reactive oxygen species (ROS) and ROS-induced ROS release. *Physiol. Rev.* **2014**, *94*, 909−950.

(24) Wang, Y.; Xu, S.; Shi, L.; Teh, C.; Qi, G.; Liu, B. Cancer-Cell-Activated in situ Synthesis of Mitochondria-Targeting AIE Photosensitizer for Precise Photodynamic Therapy. *Angew. Chem.* **2021**, *60*, 14945−14953.

(25) Yang, X.; Wang, N.; Zhang, L.; Dai, L.; Shao, H.; Jiang, X. Organic nanostructure-based probes for two-photon imaging of mitochondria and microbes with emission between 430 nm and 640 nm. *Nanoscale* **2017**, *9*, 4770−4776.

(26) Liu, C.; Hang, Y.; Jiang, T.; Yang, J.; Zhang, X.; Hua, J. A light-up fluorescent probe for citrate detection based on bispyridinum amides with aggregation-induced emission feature. *Talanta* **2018**, *178*, 847−853.

(27) Schuhmacher, C.; Gretschel, S.; Lordick, F.; Reichardt, P.; Hohenberger, W.; Eisenberger, C. F.; Haag, C.; Mauer, M. E.; Hasan, B.; Welch, J.; Ott, K.; Hoelscher, A.; Schneider, P. M.; Bechstein, W.; Wilke, H.; Lutz, M. P.; Nordlinger, B.; Van Cutsem, E.; Siewert, J. R.; Schlag, P. M. Neoadjuvant chemotherapy compared with surgery alone for locally advanced cancer of the stomach and cardia: European Organisation for Research and Treatment of Cancer randomized trial 40954. *J. Clin. Oncol.* **2010**, *28*, 5210−5218.

(28) Zhou, T.; Zhu, J.; Shang, D.; Chai, C.; Li, Y.; Sun, H.; Li, Y.; Gao, M.; Li, M. Mitochondria-Anchoring and AIE-Active Photosensitizer for Self-Monitored Cholangiocarcinoma Therapy. *Mater. Chem. Front.* **2020**, *4*, 3201−3208.

(29) Schellenberg, B.; Wang, P.; Keeble, J. A.; Rodriguez-Enriquez, R.; Walker, S.; Owens, T. W.; Foster, F.; Tanianis-Hughes, J.; Brennan, K.; Streuli, C. H.; Gilmore, A. P. Bax exists in a dynamic equilibrium between the cytosol and mitochondria to control apoptotic priming. *Mol. Cell* **2013**, *49*, 959−971.

(30) Garrido, C.; Galluzzi, L.; Brunet, M.; Puig, P. E.; Didelot, C.; Kroemer, G. Mechanisms of cytochrome c release from mitochondria. *Cell Death Differ.* **2006**, *13*, 1423−1433.

(31) Lindsten, T.; Ross, A. J.; King, A.; Zong, W. X.; Rathmell, J. C.; Shiels, H. A.; Ulrich, E.; Waymire, K. G.; Mahar, P.; Frauwirth, K.; Chen, Y.; Wei, M.; Eng, V. M.; Adelman, D. M.; Simon, M. C.; Ma, A.; Golden, J. A.; Evan, G.; Korsmeyer, S. J.; MacGregor, G. R.; Thompson, C. B. The combined functions of proapoptotic Bcl-2 family members bak and bax are essential for normal development of multiple tissues. *Mol. Cell* **2000**, *6*, 1389−1399.

(32) Datta, S. R.; Dudek, H.; Tao, X.; Masters, S.; Fu, H.; Gotoh, Y.; Greenberg, M. E. Akt phosphorylation of BAD couples survival signals to the cell-intrinsic death machinery. *Cell* **1997**, *91*, 231−241.

https://doi.org/10.1021/acsomega.2c05761
ACS Omega 2022, 7, 47912−47922

(33) Meller, R.; Schindler, C. K.; Chu, X. P.; Xiong, Z. G.; Cameron, J. A.; Simon, R. P.; Henshall, D. C. Seizure-like activity leads to the release of BAD from 14-3-3 protein and cell death in hippocampal neurons in vitro. *Cell Death Differ.* **2003**, *10*, 539−547.
(34) Szanto, A.; Bognar, Z.; Szigeti, A.; Szabo, A.; Farkas, L.; Gallyas, F., Jr. Critical role of bad phosphorylation by Akt in cytostatic resistance of human bladder cancer cells. *Anticancer Res.* **2009**, *29*, 159−164.
(35) Nisa, L.; Häfliger, P.; Poliaková, M.; Giger, R.; Francica, P.; Aebersold, D. M.; Charles, R. P.; Zimmer, Y.; Medová, M. PIK3CA hotspot mutations differentially impact responses to MET targeting in MET-driven and non-driven preclinical cancer models. *Mol. Cancer* **2017**, *16*, 93.
(36) Chao, D. T.; Korsmeyer, S. J. BCL-2 family: regulators of cell death. *Annu. Rev. Immunol.* **1998**, *16*, 395−419.
(37) Danial, N. N. BAD: undertaker by night, candyman by day. *Oncogene* **2008**, *27*, S53−S70.

https://doi.org/10.1021/acsomega.2c05761
ACS Omega 2022, 7, 47912−47922